Eur. Radiol. (2001) 11: 1220–1230
DOI 10.1007/s003300000707

NEURO

M. Wintermark
P. Maeder
J.-P. Thiran
P. Schnyder
R. Meuli

Quantitative assessment of regional cerebral blood flows by perfusion CT studies at low injection rates: a critical review of the underlying theoretical models

Received: 18 April 2000
Revised: 13 September 2000
Accepted: 14 September 2000
Published online: 16 February 2001

M. Wintermark · P. Maeder · P. Schnyder · R. Meuli (✉)
Department of Diagnostic and Interventional Radiology, University Hospital, CHUV-BH10, 1011 Lausanne, Switzerland
E-mail: reto.meuli@chuv.hospvd.ch
Phone: +41-21-3144556
Fax: +41-21-3144554

J.-P. Thiran
Signal Processing Laboratory, Swiss Federal Institute of Technology, 1015 Lausanne, Switzerland

Abstract Viability of the cerebral parenchyma is dependent on cerebral blood flow (CBF), which is usually kept in a very narrow range due to efficient autoregulation processes and can be altered in a variety of pathological conditions. An accurate method allowing for a quantitative assessment of regional cerebral blood flows (rCBF) and available for the routine clinical practice would, for sure, greatly contribute to improving the management of patients with cerebrovascular diseases. Different imaging techniques are now available to evaluate rCBF: positron emission tomography; single photon emission CT; stable-xenon CT; perfusion CT; and perfusion MRI. Each of these imaging techniques uses an indicator, with specific biological properties, and is supported by a model, which consists of a few simplifying assumptions, necessary to state and solve the equations giving access to rCBF. The obtained results are more or less reliable, depending on whether modeling hypotheses are fulfilled by the used indicator. The purpose of this article is to review the various supporting models in the assessment of rCBF, with special emphasis on perfusion CT studies at low injection rates and on iodinated contrast material used as an indicator.

Keywords Cerebral perfusion · Cerebrovascular disorders · Cardiovascular models · Spiral CT · Computer-assisted image processing

Introduction

Brain metabolism is provided almost exclusively by glucose oxidation. The high metabolic demand of the brain, associated with its inability to store energy, requires an important and stable cerebral perfusion, in order to guarantee a normal cerebral function. Mean cerebral blood flow (CBF) values range around 50 cc per 100 g and per minute. They are, however, higher in young people and lower in the elderly. Regional cerebral blood flows (rCBF) are twice or thrice superior in the gray matter, compared with those in the white matter. rCBF are increased in activated cerebral areas. The rCBF changes relating to cerebral activity modifications may reach 10–20%, and up to 40% in case of extreme metabolic conditions, such as coma or convulsion [1, 2].

Complex autoregulation processes ensure both the adjustment of rCBF to local energetic needs, determined by the activity level of local neurons and the stability of CBF despite changes in systemic arterial pressure. This rCBF autoregulation is controlled by intricate neurobiochemical mechanisms, involving sensitivity to blood pressure, blood pCO_2 and pH. Brain vascular autoregulation notably allows for a vascular dilatation when the systemic pressure tends to lower, in order to keep a constant CBF. This vascular dilatation leads in turn to an increased cerebral blood volume (CBV) [3, 4].

The rCBF alterations are encountered in a variety of pathological conditions, the most frequent being strokes. Strokes affect 500,000 patients every year in the United States and represent the third cause of death in

industrialized countries, behind cardiovascular diseases and cancers [5]. Functional transitory ischemic accidents occur when rCBF lowers below 20 cc per 100 g and per minute, whereas structural cerebral infarcts happen below 10–15 cc per 100 g and per minute for over 2–4 min. Multiple thresholds have actually been defined in various animal species and reported to describe the progressive inhibition of the various electric and metabolic activities of neurons. This inhibition is at first reversible and described as the "ischemic penumbra". It then evolves toward and finally ends in irreversible neuronal death. In the cortex, protein synthesis is inhibited below 50 cc per 100 g and per minute, whereas synaptic transmission is altered below 20 cc per 100 g and per minute. Finally, below 10–15 cc per 100 g and per minute, adenosine triphosphate (ATP) synthesis is interrupted and membrane ion pumping becomes impossible, soon leading to irretrievable neuronal structural damages. The rCBF values associated with these thresholds evolve with time, with progressive replacement of the penumbra by infarct. Neurons of some cerebral areas are very sensitive to hypoxia, such as those within the CA-1 sector of the hippocampus, whereas others, notably cortical neurons, are quite resistant [6, 7, 8, 9, 10].

Present indications for a thrombolytic therapy in strokes rely on the time interval from the beginning of the symptomatology and on the lesion extent on the native cerebral CT [5, 11, 12, 13, 14]. Knowledge of a quantitative mapping of rCBF, indicating the severity and potential reversibility of neuronal damage, would perhaps allow for the clinical use of the theoretical notion of viability thresholds and constitute an additional and worthy tool to decide whether to include or not a patient in a thrombolysis protocol. In salvageable cerebral areas, i.e., penumbra, the rCBF can indeed be identified as lowered, with a regional cerebral blood volume (rCBV) increased by autoregulation processes. Conversely, in infarcted cerebral parenchyma, autoregulation mechanisms are altered, and both rCBF and rCBV are diminished. Thrombolysis achieved in extended cerebral infarcts with limited penumbra does not only have little benefit but may also increase the risk of intracranial bleeding [15, 16].

Other endpoints in rCBF mapping are the evaluation of ischemic vasospasms following subarachnoidal hemorrhages [17, 18], the measurement of the cerebral vascular autoregulation and reserve, as well as that of a potential steal effect through an acetazolamide test [19, 20, 21, 22]. In the setting of a carotid aneurysm, a carotido-cavernous fistula or a basal skull tumor, repercussions of a carotid occlusion can be estimated through a balloon-occlusion test [23, 24].

Imaging techniques, indicators, and models

Measurement of rCBF relies on a triad, including an imaging technique, an indicator, and a model.

Different imaging techniques are available to evaluate rCBF: positron emission tomography (PET); single photon computed emission tomography (SPECT); stable-xenon CT (Fig. 1), perfusion CT, and perfusion MRI. Positron emission tomography remains limited to experimental studies, notably because of its cost and of its requirement of a cyclotron [25]. Single photon emission CT only affords a qualitative mapping of rCBF [26]. Stable-xenon CT provides accurate quantitative rCBF values, but necessitates excellent collaboration with a sometimes acutely affected patient, as well as specialized and expensive equipment. On the other hand, perfusion CT, which involves sequential acquisition of cerebral CT sections achieved on a stationary cine-mode during intravenous administration of a iodinated contrast material, can be performed in all institutions owning a spiral CT unit. It does not necessitate additional material. It is rapidly (40–50 s) and easily performed in every patient, even in children. Results are obtained within a few minutes and are thus available in the emergency settings. Perfusion MRI is a comparable and competing imaging technique with perfusion CT studies and relies on the same underlying theoretical models; however, it leads only to qualitative results, since the MR signal decrease or even cancellation after intravenous administration of gadolinium is not proportionally related to the gadolinium plasma concentration. Finally, diffusion MRI does not describe rCBF, but rather the functional condition of cerebral neurons, which is altered, for instance, by ischemia.

Each of these imaging techniques uses an indicator, defined as a substrate which has the same kinetics as a blood component – blood cells or plasma – but which additionally discloses a measurable signal or property. Indicators used to evaluate rCBF are distributed into three categories:

1. Indicators completely extracted at first pass, such as microspheres
2. Diffusible indicators, such as most of nuclear medicine indicators, stable xenon, ...
3. Indicators restrained to the cerebral vascular bed, at least at first-pass and in healthy cerebral parenchyma, such as iodinated contrast material used in perfusion CT studies and gadolinium used in perfusion MRI.

Perfusion CT studies (Fig. 2) allow definition of a contrast enhancement curve in connection with time for each pixel, the increase in CT number (Hounsfield units) being linearly related to a time–concentration curve. In the following developments, iodinated con-

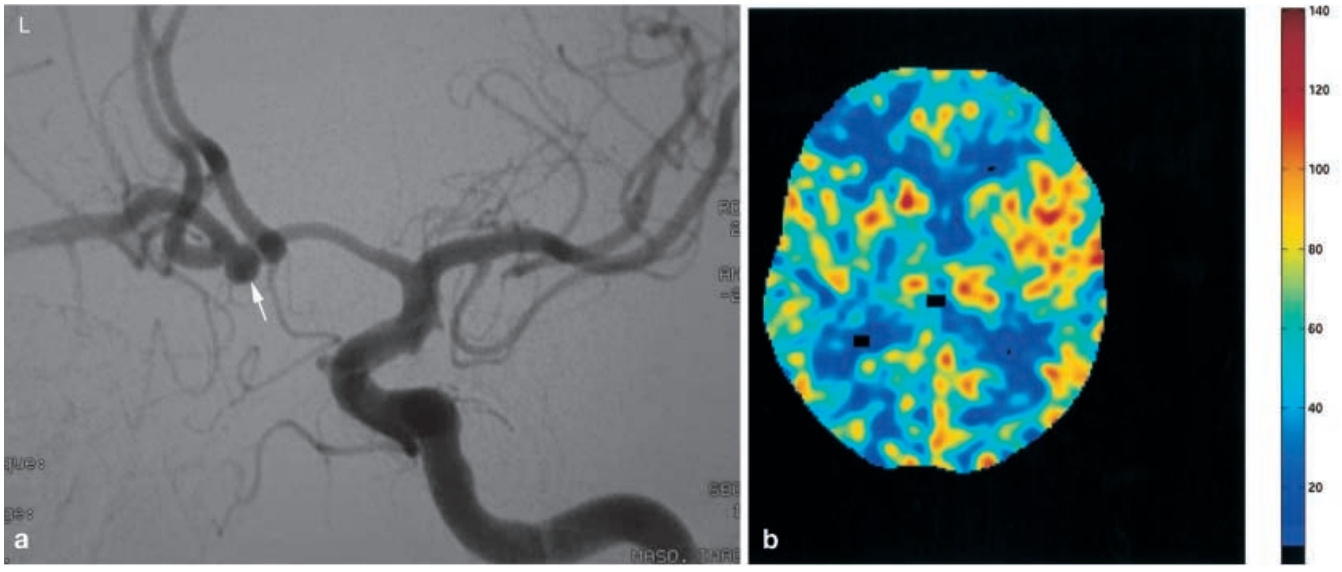

Fig. 1 a, b A 53-year-old male patient with chronic arterial hypertension who was admitted to our institution for a subarachnoid hemorrhage. **a** Lateral angiographic view relates this subarachnoid hemorrhage to a ruptured bilobulated sacciform aneurysm lying on the anterior communicant artery *(arrows)*. This aneurysm was clipped surgically. In his follow-up, the patient developed symptomatology of brain ischemia, which justified brain perfusion imaging, i.e., perfusion CT and angiographic studies. The cerebral vessels turned out to be normal. **b** Stable-xenon CT study obtained 5 min prior to the perfusion CT led to an rCBF map, which can be considered as a reference for comparison, since stable-xenon CT has been validated as an accurate and quantitative technique of rCBF measurement [79, 80, 81]

trast material concentration and contrast enhancement will be considered as equivalent (Fig. 3).

Finally, rCBF calculation is supported by a model meant to give a simplified vision of reality, i.e., a few source assumptions, necessary to state and solve the equations giving access to rCBF from the acquired images. The result thus obtained is more or less reliable, depending on whether the source hypotheses are fulfilled by the used imaging technique and indicator. Sometimes, acquisition parameters for the imaging technique are decisive. Three main models have been described:

1. The maximal slope model or model of the indicator completely extracted at first pass
2. The equilibrating indicator model
3. The central volume principle

Our purpose is a critical review of these models, with a special concern about their potential implementation to perfusion CT studies performed at low injection rates of iodinated contrast material, typically 5 cc/s.

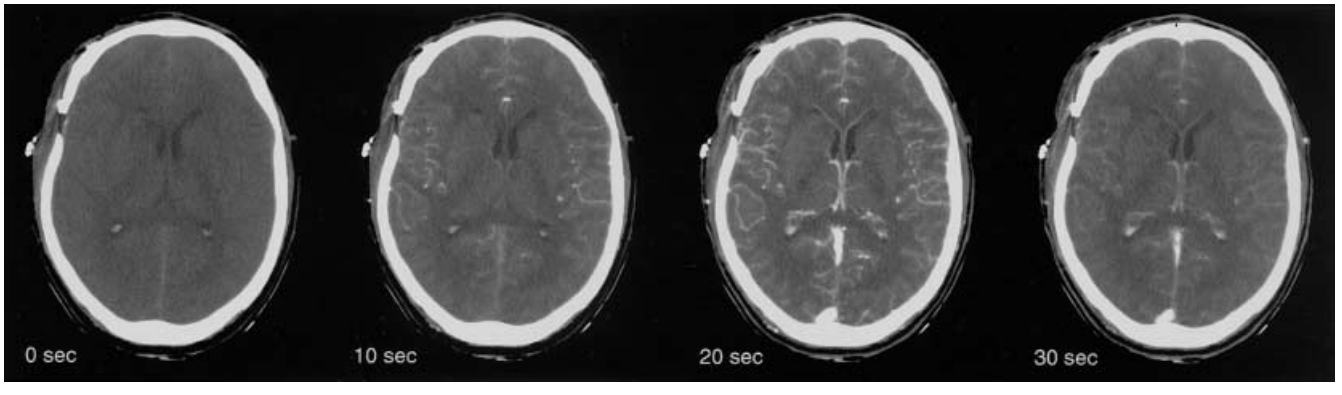

Fig. 2 Four images of the perfusion CT series realized in this patient, consisting of 25 sequential axial 10-mm CT sections obtained every 2 s at these two adjacent levels due to multidetector array technology, with a total acquisition time of 50 s. Acquisition parameters were 80 kVp and 200 mAs. The CT scanning was initiated 2 s prior to intravenous administration of 90 cc of iodinated contrast material at a rate of 5 cc/s

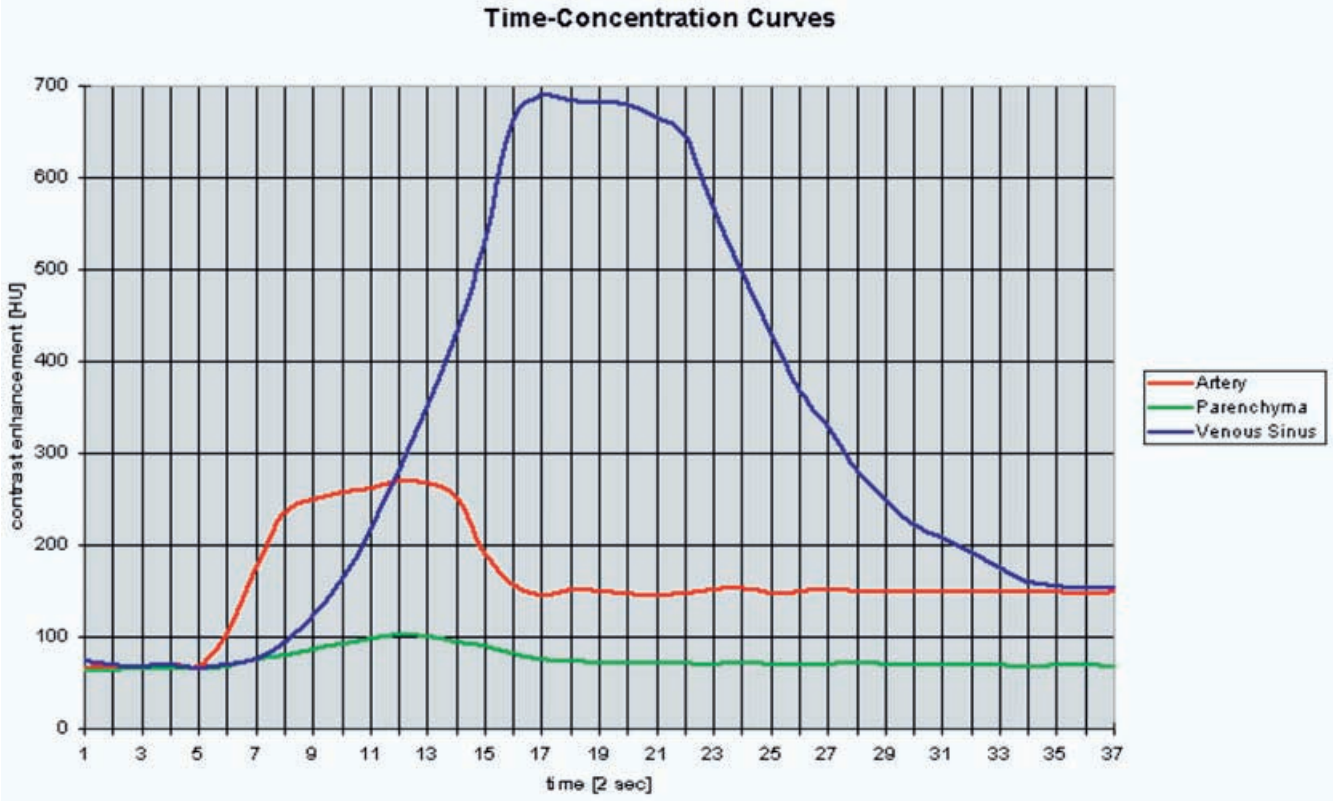

Fig. 3 Time–concentration curves obtained from the patient's perfusion CT series in an arterial pixel, in a parenchymal pixel, and in a pixel at the center of the superior sagittal venous sinus, respectively. Contrast enhancement in Hounsfield units is considered with respect to time expressed in steps of 2 s. Two elements are noteworthy: Firstly, contrast enhancement is more marked in the venous pixel than in the arterial and parenchymal pixels, due to the different sizes of the corresponding vessels, with, as a result, a more or less important partial-volume averaging effect. Secondly, the parenchymal time–concentration curve compared with the arterial curve, and the venous time–concentration curve compared with the parenchymal curve, show more and more flattened profiles as well as more and more delayed peak with regard to time. This relates to the iodinated contrast material first traveling in arteries, then in parenchymatous capillaries and finally in veins

Maximal slope model

The maximal slope model was initially described for microspheres, whether colored or radiolabelled. Intra-arterially injected microspheres are distributed in the various arterial territories proportionally to the blood flows irrigating them. They are trapped in the precapillary or capillary networks and are thus said to be completely extracted at first pass. The total amount of microspheres accumulated in a given area is proportional to its perfusion, as well as to the rate of accumulation of the microspheres, i.e., to the slope of the accumulation curve.

From a mathematical point of view, the number of "extracted" microspheres $Q(t)$ in a local vascular network in connection with time t can be described, according to the Fick principle, by the equation:

$$\frac{dQ(t)}{dt} = rCBF * C_a(t) \tag{1}$$

where $C_a(t)$ designates the instantaneous arterial concentration of microspheres at time t.

The rCBF can then be expressed as:

$$rCBF = \frac{\frac{dQ(t)}{dt}}{C_a(t)} \tag{2}$$

Equation (2) finds one particular application for the maximal values of numerator and denominator:

$$rCBF = \frac{maximal\ slope\ of\ Q(t)}{maximal\ height\ of\ C_a(t)} \tag{3}$$

[27, 28, 29].

The maximal slope model can be applied to perfusion CT studies. However, iodinated contrast material is not completely extracted at first pass. Thus, in order to mimic a complete extraction of the iodinated contrast material at first pass, use of low injection rates necessitates not to consider the instantaneous contrast enhancement, but to add up successive measurements of

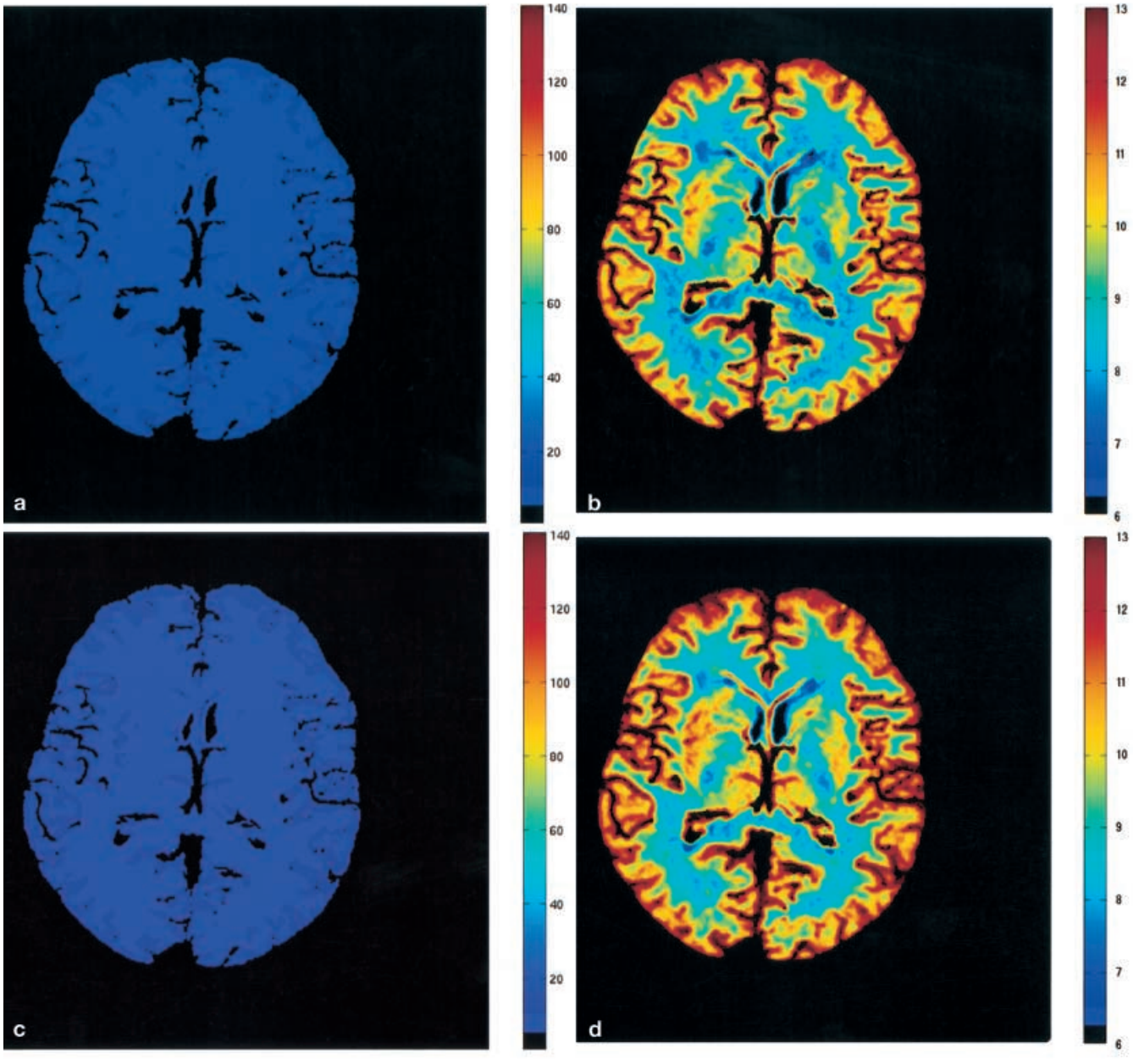

Fig. 4a–d Maximal slope model rCBF maps (cubic centimeters per 100 g and per minute), the slope in each pixel being divided by that in **a,b** an arterial or **c,d** a venous pixel. The maximal slope model considers the total accumulated contrast enhancement in a given area to be proportional to its perfusion, i.e., to its rCBF, as well as to the rate of accumulation of the contrast material, i.e., to the slope of the accumulation curve. **a,b** The calculation of the final rCBF necessitates a reference arterial pixel. Time–concentration curves in arterial pixels necessitate a correction for partial-volume averaging. **c,d** Some authors thus prefer to choose, as a reference, the pixel at the center of the superior sagittal venous sinus, which is free from partial-volume averaging, even if the maximal slope in this venous pixel is different from the one in an artery. **a,c** Both rCBF maps, which are displayed with the same color map (0–140 cc per 100 g and per minute), underestimate absolute values of rCBF. **b,d** As demonstrated with a dedicated color map, they do not show the contrast between gray and white matter perfusion, which is expected to be in the range of two to three, whatever the arterial or venous reference pixel

contrast enhancement along with time, so as to rebuild an accumulation curve *Q(t)* [30, 31, 32, 33].

In order to be valid, this model necessitates a very short injection time and thus a very high injection rate for the intravenous administration of contrast material. If the injection rate is too low, fractions of contrast enhancement are missed and rCBF values thus underestimated. This rCBF underestimation has also been reported when contrast material is injected at injection rates as high as 20 cc per second, for brain perfusion [32, 33] and for kidney and spleen perfusion [30, 31]. The rCBF underestimation is even higher (Fig. 4a,c) when the injection rate is 5 cc/s, the latter being the maximal

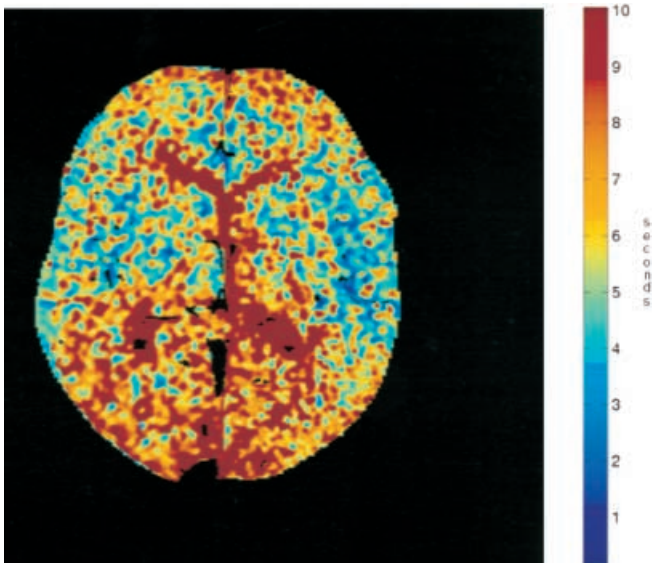

Fig. 5 Central volume principle mean transit time (MTT) map (seconds) is obtained through a non-parametric deconvolution. Deconvolution is a memory operation which allows determination of the behavior of a unique and instantaneous unit bolus of iodinated contrast material crossing the parenchymal capillary network. It allows notably calculation of the mean time spent by this instantaneous contrast material bolus to cross the capillary network, which relates to the MTT

injection rate bearable by patients in the setting of an intravenous administration of iodinated contrast material at the level of a small peripheric vein. Moreover, with an injection rate of 5 cc/s, the contrast between gray matter and white matter perfusion (expected in the range of 2–3) is not demonstrated (Fig. 4c,d). This probably relates to the relatively high and low blood flows in the gray and the white matter, respectively, thus resulting in an increase of missed fractions of contrast enhancement by the sequential CT acquisition and in greater rCBF underestimation in the gray matter than in the white matter.

Finally, the arterial pixel chosen as a reference for the denominator in Eq. (3) (Fig. 4a,b) is often affected by partial-volume averaging and thus necessitates adequate correction. Some authors therefore prefer to consider the pixel at the center of the superior sagittal venous sinus as a reference (Fig. 4c,d), because this sinus is free from partial-volume averaging, even if the maximal slope in this venous pixel is different from that in an artery [32, 33].

Mean transit time and rCBV

The equilibrating indicator model and the central volume principle both involve the notion of mean transit time (MTT) resulting from a mathematical operation called deconvolution.

The profile of the time–concentration curve $C_b(t)$ in each pixel of the cerebral parenchyma can be derived from the profile of the time–concentration curve $C_a(t)$ in the supplying artery through a convolution operation. Convolution is a "memory operation" which considers the arterial time–concentration curve at the input of the vascular system as a sum of successive contrast material boluses. Every one of these boluses is modified during its passage through the vascular network and they finally superpose, shifted in time, to create the time–concentration curve at the output of the vascular system. Convolution describes the current parenchymal concentration of the indicator (at time t) as a function of the current and previous arterial concentrations:

$$C_b(t) = C_a(t) \otimes h(t) = \int_{s=0}^{t} (C_a(t-s) * h(s) * ds) \quad (4)$$

Conversely, knowledge of the parenchymal and arterial time–concentration curves allows for an inverse operation, or deconvolution, the result of which is an "impulse function" $h(t)$. This impulse function $h(t)$ describes the parenchymal time–concentration curve that would theoretically be obtained in case of intra-arterial administration of a unique and instantaneous unit bolus of iodinated contrast material. The impulse function $h(t)$ depends both on the anatomical characteristics of the regional vascular networks and on the behavior of the indicator. The impulse function $h(t)$ has a certain time extent, from a minimum to a maximum, relating to the range of transit times of the indicator through various-length pathways within the regional vascular network. From the impulse function $h(t)$ can be derived an MTT (Fig. 5), which is defined as the weighted mean of the transit-time distribution:

$$MTT = \int_{t=0}^{\infty} h(t) * t * dt \quad (5)$$

In addition to the MTT, the rCBV is the second parameter to be determined. The rCBV designates the fraction within cerebral tissue that is occupied by blood vessels and its unit is cubic centimeters per 100 g. Typical rCBV values are 5–6 cc per 100 g for the gray matter and 2–3 cc per 100 g for the white matter.

The rCBV calculation from perfusion CT studies (Fig. 6) relies on the partial-volume averaging effect. Axel [34] indeed readily demonstrated that the time–concentration curves in arterial, parenchymal, and venous pixels have various profiles, as explained previously, but should theoretically always have the same area under the curve, according to the mass-conservation principle; however, contrast enhancement only involves the vascular volume. Time–concentration curves measured during perfusion CT studies do therefore not all have the same area: they are more marked in pure vascular pixels than in parenchymal pixels including

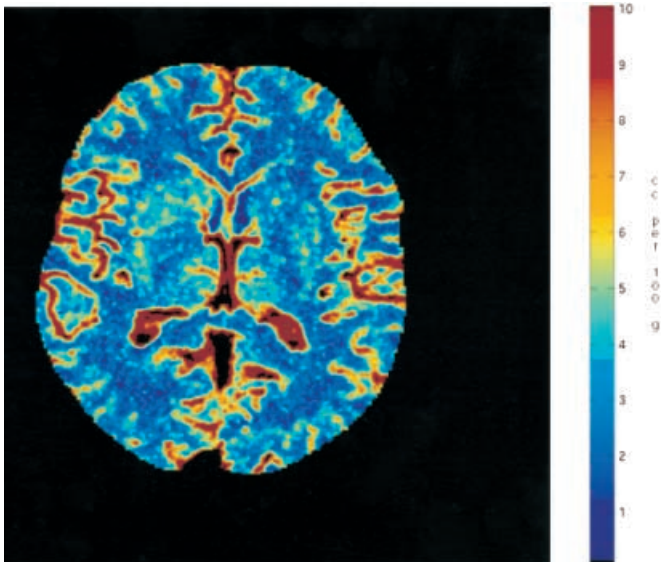

Fig. 6 This rCBV map (cubic centimeters per 100 g) is inferred from a quantitative assessment of the partial-volume averaging in each pixel. Contrast enhancement involves only the vascular volume indeed. As seen in Fig. 3, time–concentration curves measured in vivo during perfusion CT studies are thus more marked in pure vascular pixels than in pixels including blood within capillaries but also neurons, axonal tubes, and myelin sheaths, where the vascular volume represents only a few percent of the total tissue volume, thus leading to a partial-volume averaging effect. This partial-volume effect can be exploited to determine information about the fraction of vascular volume within the total tissue volume and to infer an rCBV map. Calculation of rCBV map necessitates knowledge of the contrast enhancement profile in a reference pixel devoid of partial-averaging effect. This pixel is usually chosen at the center of the superior sagittal venous sinus

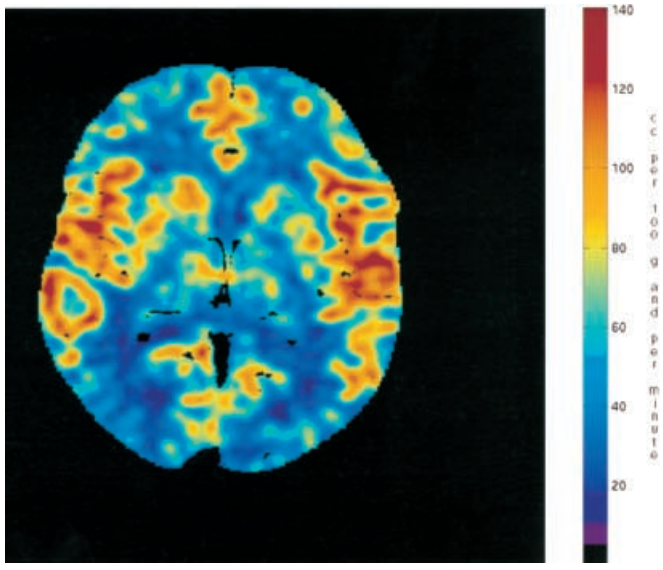

Fig. 7 Central volume principle rCBF map (cubic centimeters per 100 g and per minute) is obtained by dividing the rCBV map by the MTT map: blood flow is only blood volume considered with respect to time. The central volume principle rCBF map is displayed with the same color map (0–140 cc per 100 g and per minute) as in Fig. 4a,b, thus allowing for comparisons between the various model analyses. Central volume principle rCBF map displays absolute rCBF values which, in healthy cerebral areas, match those reported in the literature. Moreover, it outlines contrast between gray and white matter

blood within capillaries but also neurons, axonal tubes, and myelin sheaths, for which the vascular volume only represents a few percent of the total tissue volume, thus leading to a partial-volume averaging effect. This partial-volume effect can be used to deduce information from the fraction of vascular volume within the total tissue volume and to infer a rCBV map. Calculation of a rCBV map necessitates knowledge of the contrast enhancement profile in a reference pixel devoid of partial-averaging effect. This pixel must be completely surrounded by a rim of vascular pixels, such as, for instance, at the center of the superior sagittal venous sinus, which can always be identified on axial cerebral CT sections [35, 36, 37, 38]:

$$rCBV = \frac{\textit{area under the curve in a parenchymal pixel}}{\textit{area under the curve in the reference pixel}} \tag{6}$$

More precisely, since iodinated contrast material only mixes up with blood plasma, the values of the above-obtained map must be divided by the hematocrit in order to obtain the real rCBV. The hematocrit taken into account is not the one within large vessels, but the microhematocrit. Due to its variation in the various cerebral areas, a mean value – typically 0.85 of the venous macrohematocrit – is classically used [39, 40].

Finally, since the rCBV designates a blood volume, whereas the MTT relates to the time taken by the blood to cross the local capillary network, their combination through a simple relationship leads to the rCBF (Fig. 7), which amounts to nothing but a flow, i.e., a blood volume per time unit [34, 35]:

$$rCBF = \frac{rCBV}{MTT} \tag{7}$$

Note that some authors, instead of using the impulse function, prefer the notion of residue function [41]. Whereas the impulse function relates to the contrast material arriving and leaving the vascular network, the residue function describes the elimination process of the contrast medium once it has entered in the vascular system. Impulse and residue functions relate to different aspects of the same phenomenon and lead to identical results.

Equilibrating indicator model

The equilibrated indicator model was initially described by Zuntz [42] and von Schrotter [43] and extensively applied to anesthetic gases by Kety [44] and Kety and Schmidt [45], who deduced the global CBF from successive femoral arterial and jugular venous samplings and corresponding concentrations of nitrous oxide (NO).

The equilibrating indicator basically relies on the Fick principle:

$$\frac{dQ(t)}{dt} = rCBF * (C_a(t) - C_v(t)) \tag{8}$$

where $C_a(t)$ and $C_v(t)$ designate the instantaneous arterial and venous concentration of the indicator at time t, whereas $Q(t)$ designates the amount of indicator in the local vascular networks in connection with time t. $Q(t)$ can be described as the product of the arterial volume and the arterial concentration, as the product of the venous volume and the venous concentration or as the product of the local capillary volume rCBV and the parenchymal concentration $C_b(t)$:

$$Q(t) = \text{rCBV}^* C_b(t) \tag{9}$$

The equilibrating indicator model supposes a balance between the venous – $C_v(t)$ – and the parenchymal – $C_b(t)$ – concentrations of the indicator:

$$C_b(t) = \lambda \, ^* C_v(t) \tag{10}$$

where λ relates to the cerebral parenchyma–blood partition coefficient of the indicator.

Combination and development of Eqs. (8), (9), and (10) result in the supporting equation of the equilibrating indicator model [49, 50, 51]:

$$C_b(T) = \lambda * K * \int_{t=0}^{T} C_a(t) * e^{-K*(T-t)} * dt \tag{11}$$

with

$$K = \frac{rCBF}{\lambda} \tag{12}$$

This equation means that a balance of the indicator concentrations between blood and cerebral parenchyma is more or less rapidly realized in the various cerebral areas according to the importance of the corresponding rCBF. Knowledge of the arterial and parenchymal concentration curves leads to the balance rates and the rCBF for each pixel [44, 46].

The equilibrating indicator model applies mainly to diffusible indicators, such as those used in nuclear medicine [47], and for stable-xenon CT (Fig. 1b) [48, 49, 51].

Central volume principle

The central volume principle was developed by Stewart and Hamilton. Stewart experienced intravenous administration of saline solutions on anesthetized animals and measured changes of electrical blood conductance in various vascular sites. He also performed dye injection with color recording in the retinal vessels at the eye fundus [52, 53, 54, 55, 56, 57]. Hamilton et al. improved the concept of time–concentration curves [58, 59, 60, 61]. Meier and Zierler then applied the model developed by Stewart and Hamilton to the measurement of regional blood flows [62, 63, 64]. Finally, Axel used previously defined concepts in the setting of dynamic CT measurements of local perfusion [34, 35, 65].

The central volume principle is the most general model, with the fewest source hypotheses. It considers regional vascular networks as isolated volumes, each with both an arterial input and a venous output. It assumes that the whole amount of an indicator introduced at some time in the isolated volume will leave it sooner or later. As explained previously, the output time–concentration curve can be described as a convolution between the input time–concentration curve and the impulse function. The key of the central volume principle lies in solving the inverse operation, i.e., the deconvolution of the measured parenchymal and arterial time-curve concentration profiles, which leads to the impulse response and, in turn, to MTT and, combined with rCBV, to rCBF [66, 67, 68].

The deconvolution process can be realized in two ways. The first method, called parametric deconvolution, consists of admitting supplemental hypotheses with regard to the anatomical structure or to the behavior of the indicator. The shape of the impulse function, i.e., its parametric equation, can be derived from these hypotheses. Deconvolution then consists in finding the parameters of the equation so that the convolution of this impulse function with the arterial time–concentration curve optimally fits the parenchymal time–concentration curve. The central volume can be simplified as a rectangle, with the indicator moving as if pushed by a piston: a rectangular impulse function is used for such iterations. The central volume can be seen as a network of parallel capillaries, the lengths of which are distributed according to a gaussian law: the associated impulse function has a gaussian shape. Finally, the indicator can be considered in an equilibration process between the blood and the total volume in which it will distribute, as assumed in the equilibrating indicator model: the impulse function is then a decreasing exponential curve. The second technique to solve a deconvolution is non-parametric, meaning that no additional assumptions are required regarding the anatomy or physiology of the central volume, which are always hypothetical and may not apply to the physiological reali-

ty. Classical non-parametric solutions are obtained either by single value deconvolution [41] or by least-mean-square deconvolution. Non-parametric deconvolution, which involves less source hypotheses, leads to better results than parametric deconvolution [69].

Applying the central volume principle to perfusion CT studies necessitates to correction of time–concentration curves for recirculation, since the model considers the vascular networks with a single input, a single output, and no communication between them. Recirculating contrast material could theoretically be considered as a second injected bolus. However, contrast enhancement associated with it is lower and thus more altered by noise, and deconvolution is known to be very sensitive to noise. Thus, time–concentration curves have to be corrected for recirculation, e.g., through a gamma-variate fitting.

Iodinated contrast material can be considered to remain intravascular in cerebral capillaries, at least at first pass and in healthy cerebral regions [70, 71, 72, 73]. A correction method has been reported for the extravasation of contrast material in pathological areas [74].

Analysis of perfusion CT data according to the central volume principle (Fig. 7) leads to rCBF values in agreement with those reported in the literature. Contrast between gray and white matter is outlined [75, 76, 77].

On the other hand, estimated rCBF in pixels, including cerebral parenchyma but also arterial vessels, is high, since blood flow in cerebral vessels is much greater than in cerebral parenchymal capillaries. Since the rCBF map should ideally display only capillary blood flows, values obtained in pixels including arterial vessels are overestimated [75, 76, 77].

Practical implementation of the central volume principle to perfusion CT studies

Perfusion CT studies are achieved at our institution according to the following protocol: 25 sequential axial 10-mm CT sections are acquired every 2 s at two adjacent levels due to the multidetector array technology, with a total acquisition time of 50 s. Acquisition parameters are 80 kVp and 200 mAs. The CT scanning is initiated 2 s prior to intravenous administration of 90 cc (1.3 cc/kg) of iodinated contrast material at a rate of 5 cc/s (Fig. 2). The choice of 80 kVp is justified by an increased contrast enhancement and a reduced patient irradiation at such kilovoltage.

Perfusion CT data are transferred to a workstation and analyzed through a commercial software or through a software that we developed and will soon be available as a freeware [78]. Perfusion CT data consist of contrast enhancement profiles obtained at each pixel. These profiles relate linearly to time–concentration curves of the contrast material (Fig. 3). Improvement of the signal-to-noise ratio is performed through spatial filtering (5-by-5 mean filter) of the parenchymal contrast enhancement profiles. These profiles are then corrected for recirculation through a gamma-variate fitting. Analysis of these curves is performed according to the central volume principle. The reference arterial pixel is chosen as the one with the shorter time to peak. The rCBV map (Fig. 6) results from a quantitative estimation of the partial-volume averaging effect, completely absent in a reference pixel at the center of the large superior sagittal venous sinus, according to Eq. (6). A correction factor takes into consideration that iodinated contrast material is restricted to the plasma phase of the blood. The impulse function and the relating MTT map (Fig. 5) are inferred from a deconvolution of the parenchymal time–concentration curves by a reference arterial one using the least-mean-square deconvolution method, which is known to be efficient and stable (Other deconvolution methods are also available, such as the singular value decomposition one). Finally, combination of rCBV and MTT at each pixel leads to an rCBF value (Fig. 7) through Eq. (7).

Conclusion

Knowledge of the rCBF would for sure be a worthy contribution to the management of patients with cerebrovascular disease. An rCBF map is obtained by several imaging techniques, among which are perfusion CT studies, which are simple and easy to perform, even in acute patients. Perfusion CT data involve intravenous administration of iodinated contrast material and can be analyzed according to various models. For low injection rates of iodinated contrast material, the best model is the central volume principle with a non-parametric deconvolution, since it involves the least assumptions about cerebral hemodynamics, and thus the least potential pitfalls. It leads to rCBF values matching those reported in the literature. It outlines the contrast between gray and white matter, and between healthy and pathological cerebral parenchyma. It does not necessitate high injection rates, which are not acceptable in patients.

References

1. Reivich M (1974) Blood flow metabolism couple in brain. Res Pub Assoc Res Nerv Ment Dis 53: 125–140
2. Lassen NA (1959) Cerebral blood flow and oxygen consumption in man. Physiol Rev 39: 183–238
3. Harper AM (1966) Autoregulation of cerebral blood flow: influence of the arterial blood pressure on the blood flow through the cerebral cortex J Neurol Neurosurg Psychiatry 29: 398–403
4. Wood JH (1987) Cerebral blood flow: physiologic and clinical aspects. McGraw-Hill, New York
5. National Institute of Neurological Disorders and Stroke (NINDS) rt-PA Stroke Study Group (1995) Tissue plasminogen activator for acute ischaemic stroke. N Engl J Med 333: 1581–1587
6. Symon L, Branston NM, Strong AJ, Hope TD (1977) The concepts of thresholds of ischaemia in relation to brain structure and function. J Clin Pathol 30 (Suppl):149–154
7. Astrup J, Symon L, Siesjö BK (1981) Thresholds in cerebral ischemia: the ischemic penumbra. Stroke 12: 723–725
8. Hakim AM (1987) The cerebral ischemic penumbra. Can J Neurol Sci 14: 557–559
9. Hossman KA (1994) Neuronal survival and revival during and after cerebral ischemia. Am J Emerg Med 1: 191–197
10. Hossmann KA (1994) Viability thresholds and the penumbra of focal ischemia. Ann Neurol 36: 557–565
11. Hacke W, Kaste M, Fieschi C (1995) Intravenous thrombolysis with recombinant tissue plasminogen activator for acute hemispheric stroke. The European Cooperative Acute Stroke Study (ECASS). J Am Med Assoc 274: 1017–1025
12. Jansen O (1995) Thrombolytic therapy in acute occlusion of the intracranial internal carotid artery bifurcation. Am J Neuroradiol 16: 1977–1986
13. Hacke W, Kaste M, Fieschi C (1998) Randomised double-blind trial placebo-controlled trial of thrombolytic therapy with intravenous therapy with intravenous alteplase in acute ischaemic stroke (ECASS II). Lancet 352: 1245–1251
14. Hennerici M (1999) Improving the outcome of acute stroke management. Hosp Med 60: 44–49
15. Sorensen AG, Copen WA, Ostergaard L et al. (1999) Hyperacute stroke: simultaneous measurement of relative cerebral blood volume, relative cerebral blood flow, and mean tissue transit time. Radiology 210: 519–527
16. Ezura M, Takahashi A, Yoshimoto T (1996) Evaluation of regional cerebral blood flow using single photon emission tomography for the selection of patients for local fibrinolytic therapy of acute cerebral embolism. Neurosurg Rev 19: 231–236
17. Powers WJ, Grubb RL, Baker RP et al. (1985) Regional cerebral blood flow and metabolism in reversible ischemia due to vasospasm: determination by positron emission tomography. J Neurosurg 62: 539–546
18. Fukui MB, Johnson DW, Yonas H, et al. (1992) Xe/CT cerebral blood flow evaluation of delayed symptomatic cerebral ischemia after subarachnoid hemorrhage. Am J Neuroradiol 13: 265–270
19. Rogg J, Rutigliano M, Yonas H, Johnson DW et al. (1989) The acetazolamide challenge: imaging techniques designed to evaluate cerebral blood flow reserve. Am J Neuroradiol 10: 803–810
20. Rutigliano MJ, Yonas H, Johnson DW (1989) Natural history of patients with compromised cerebral reserves. J Cereb Blood Flow Metab 9:S609
21. Okabe T, Meyer JS, Okayasu H (1986) Xenon-enhanced CT CBF measurements in cerebral steal in patients with arteriovenous malformation. Arch Neurol 43: 779–785
22. Marks MP, O'Danahue J, Fabricant JI et al. (1990) Cerebral blood flow evaluation of arteriovenous malformations with stable xenon CT. Am J Neuroradiol 11: 441–448
23. De Vries EJ, Sekhar LN, Horton JA et al. (1990) A new method to predict safe resection of the internal carotid artery. Laryngoscope 100: 85–88
24. Erba SM, Horton JA, Latchaw RE et al. (1988) Balloon test occlusion of the internal carotid artery with stable xenon/CT cerebral blood flow imaging. Am J Neuroradiol 9: 533–538
25. Iida H, Jones T, Miura S (1998) Noninvasive quantitation of cerebral blood flow using oxygen-15-water and a dual-PET system. J Nucl Med 39: 1789–1798
26. Ito H, Iida H, Bloomfield PM et al. (1995) Rapid calculation of regional cerebral blood flow and distribution volume using iodine-123-iodoamphetamine and dynamic SPECT. J Nucl Med 36: 531–536
27. Heymann MA, Payne BD, Hoffman JIE, Rudolph Am (1977) Blood flow measurements with radionuclide-labeled particles. Prog Cardiovasc Dis 20: 55–79
28. Peters AM, Brown J, Hartnell GG et al. (1978) Non-invasive measurement of renal blood flow with ^{99m}Tc DTPA: a comparison with radiolabelled microspheres. Cardiovasc Res 21: 830–834
29. Peters AM, Gunasekera RD, Henderson BL et al. (1987) Non-invasive measurements of blood flow and extraction fraction. Nucl Med Commun 8: 823–837
30. Miles KA (1991) Measurement of tissue perfusion by dynamic computed tomography. Br J Radiol 64: 409–412
31. Bell SD, Peters AM (1991). Measurement of blood flow from first-pass radionuclide angiography: influence of bolus volume. Eur J Nucl Med 18: 885–888
32. König M, Klotz E, Heuser L (1998) Perfusion CT in acute stroke: characterization of cerebral ischemia using parameter images of cerebral blood flow and their therapeutic relevance. Clinical experiences. Electromedica 66: 61–67
33. König M, Klotz E, Luka B et al. (1998) Perfusion CT of the brain: diagnostic approach for early detection of ischemic stroke. Radiology 209: 85–93
34. Axel L (1980) Cerebral blood flow determination by rapid-sequence computed tomography. Radiology 137: 679–686
35. Axel L (1981) A method of calculating brain blood flow with a CT dynamic scanner. Adv Neurol 30: 67–71
36. Ladurner G, Zilkha E, Iliff LD et al. (1976) Measurement of regional cerebral blood volume by computerized axial tomography. J Neurol Neurosurg Psychiatry 39: 152–155
37. Zilkha E, Ladurner G, Linette D et al. (1976) Computer subtraction in regional cerebral blood-volume measurements using the EMI-scanner. Br J Radiol 49: 330–334
38. Ladurner G, Zikha E, Sager WD et al. (1979) Measurement of regional cerebral blood volume using the EMI 1010 scanner. Br J Radiol 52: 371–374
39. Larson OA, Lassen NA (1964) Cerebral hematocrit in normal man. J Appl Physiol 19: 571–574
40. Sakai F, Kakazawa K, Tazaki Y et al. (1985) Regional cerebral blood volume and hematocrit measured in human volunteers by single-photon emission tomography. J Cereb Blood Flow Metab 5: 207–213
41. Ostergaard L, Sorensen AG, Kwong KK et al. (1996) High resolution measurement of cerebral blood flow using intravascular tracer bolus passages. Part I. Mathematical approach and statistical analysis. Magn Reson Med 36: 715–725

42. Zuntz N (1897) Zur Pathogenese und Therapie der durch rasche Luftdruckänderungen erzeugten Krankenheiten. Fortschr Med 15: 632–639
43. Schrotter H von (1906) Der Sauerstoff in der Prophylaxe und Therapie der Luftdruckerkrankungen in Michaelis M. Handbuch der Sauerstofftherapie. Hirschwald, Berlin
44. Kety SS (1951) The theory and applications of the exchange of inert gas at the lungs and tissues. Pharmacol Rev 3: 1–41
45. Kety SS, Schmidt CF (1948) The nitrous oxide method for the quantitative determination of cerebral blood flow in man: theory, procedure and normal values. J Clin Invest 27: 476–483
46. Jacquez AA (1985) Compartmental analysis in biology and medicine, 2nd edn. University of Michigan Press, Ann Arbor
47. Sakurada O, Kennedy C, Jehle J et al. (1978) Measurement of local cerebral blood flow with iodo[^{14}C]antipyrine. Am J Physiol 234:H59–H66
48. Winkler SS, Sacket JF, Holden JE et al. (1977) Xenon inhalation as an adjunct to computerized tomography of the brain: preliminary study. Invest Radiol 12: 15–18
49. Kelcz F, Hilal SK, Hartwell P, Joseph PM (1978) Computed tomographic measurement of the xenon brain-blood partition coefficient and implications for regional cerebral blood flow: a preliminary report. Radiology 127: 385–392
50. Drayer BP, Wolfson SK Jr, Reinmuth OM et al. (1978) Xenon enhanced computed tomoraphy for the analysis of cerebral integrity, perfusion and blood flow. Stroke 9: 123–130
51. Yonas H, Darby JM, Marks EC et al. (1991) CBF measured by Xe-CT: approach to analysis and normal values. J Cereb Blood Flow Metab 17: 716–725
52. Stewart GN (1894) Researches on the circulation time in organs and on the influences which affect it. J Physiol 15: 1–89
53. Stewart GN (1897) Researches on the circulation time and on the influence which affect it. IV. The output of heart. J Physiol 22: 159–183
54. Stewart GN (1897) The measurement of the output of the heart. Science 5: 137
55. Stewart GN (1921) The output of the heart in dogs. Am J Physiol 57: 27–50
56. Stewart GN (1921) The pulmonary circulation time, the quantity of blood in the lungs and the output of the heart. Am J Physiol 58: 20–44
57. Stewart GN (1921) Researches on the circulation time and on the influences which affect it. V. The circulation time of the spleen, kidney, intestine, heart (coronary circulation) and retina, with some further observations on the time of the lesser circulation. Am J Physiol 58: 278–295
58. Hamilton WF, Moore JW, Kinsman JM, Spurling RG (1928) Simultaneous determination of the pulmonary and systemic circulation times in man and of a figure related to the cardiac output. Am J Physiol 84: 338–344
59. Hamilton WF, Moore JW, Kinsman JM, Spurling RG (1928) Simultaneous determination of the greater and lesser circulation times, of the mean velocity of blood flow through the heart and lungs, of the cardiac output and an approximation of the amount of blood actively circulating in the heart and lungs. Am J Physiol 85: 377–378
60. Hamilton WF, Moore JW, Kinsman JM, Spurling RG (1932) Studies on the circulation. IV. Further analysis of the injection method, and of changes in hemodynamics under physiological and pathological conditions. Am J Physiol 99: 534–551
61. Hamilton WF, Riley AM, Attyah AM et al. (1948) Comparison of the Fick and dye injection methods of measuring the cardiac output in man. Am J Physiol 153: 309–321
62. Meier P, Zierler KL (1954) On the theory of the indicator-dilution method for measurement of blood flow and volume. J Appl Physiol 12: 731–744
63. Zierler KL (1962) Theoretical basis of indicator-dilution methods for measuring flow and volume. Circ Res 10: 393–407
64. Zierler KL (1965) Equations for measuring blood flow by external monitoring of radioisotopes. Circ Res 16: 309–321
65. Axel L (1983) Tissue mean transit time from dynamic computed tomography by a simple deconvolution technique. Invest Radiol 18: 94–99
66. Kinsman JM, Moore JW, Hamilton WF (1929) Studies on the circulation. I. Injection method: physical and mathematical considerations. Am J Physiol 89: 322–330
67. Stephenson JL (1948) Theory of the measurement of blood flow by the dilution of an indicator. Bull Math Biophys 10: 117–121
68. Antman S (1975) Foundations of indicator-dilution theory. In: Bloomfield DA (ed) Dye curves: the theory and practice of indicator dilution. HM+M Medical and Scientific Publishers, Aylesbury, Bucks, England, pp 21–40
69. Ostergaard L, Sorensen AG, Kwong KK et al. (1996) High resolution measurement of cerebral blood flow using intravascular tracer bolus passages. Part II. Experimental comparison and preliminary results. Magn Reson Med 36: 726–736
70. Gado MH, Phelps ME, Coleman RE (1975) An extravascular component of contrast enhancement in cranial computed tomography. Part I. The tissue–blood ratio of contrast enhancement. Radiology 117: 589–593
71. Hindmarsh T (1975) Elimination of water-soluble contrast media from the sub-arachnoid space. Investigation with computed tomography. Acta Radiol 346: 45–50
72. Phelps ME, Kuhl DE (1976) Pitfalls in the measurement of cerebral blood volume with computed tomography. Radiology 121: 375–377
73. Newhouse JH (1977) Fluid compartment distribution of intravenous iothalamate in the dog. Invest Radiol 12: 364–367
74. Lawrence KS, Lee TY (1988) An adiabatic approximation to the tissue homogeneity model for water exchange in the brain. I. Theoretical derivation. J Cereb Blood Flow Metab 18: 1365–1377
75. Cenic A, Nabavi DG, Craen RA et al. (1999) Dynamic CT measurement of cerebral blood flow: a validation study. Am J Neuroradiol 20: 63–73
76. Nabavi DG, Cenic A, Dool J et al. (1999) Quantitative assessment of cerebral hemodynamics using CT: stability, accuracy, and precision studies in dogs. J Comput Assist Tomogr 23: 506–515
77. Nabavi DG, Cenic A, Craen RA et al. (1999) CT assessment of cerebral perfusion: experimental validation and initial clinical experience. Radiology 213: 141–149
78. Web site of the Department of Diagnostic and Interventional Radiology, Centre Hospitalier Universitaire Vaudois (CHUV): http://www.hospvd.ch/public/chuv/rad/home.htm
79. Fatouros PP, Wist AO, Kishore PRS (1987) Xenon/computed tomography cerebral blood flow measurements: methods and accuracy. Invest Radiol 22: 705–712
80. DeWitt DS, Fatouros PP, Wist AO et al. (1989) Stable xenon versus radiolabeled microsphere cerebral blood flow measurements in baboons. Stroke 20: 1716–1723
81. Gur D, Yonas H, Jackson DL et al. (1985) Simultaneous measurements of cerebral blood flow by the xenon/CT method and the microsphere method: a comparison. Invest Radiol 20: 672–677